LANGMUIR

pubs.acs.org/Langmuir Article

Structural Insights into Polymer-Bounded Lipid Nanodiscs

Ralph Maier,[†] Rodrigo Cuevas Arenas,[†] Fajun Zhang,* Ana García-Sáez, and Frank Schreiber

Cite This: *Langmuir* 2023, 39, 2450−2459 Read Online

ACCESS | Metrics & More | Article Recommendations | Supporting Information

ABSTRACT: Membrane proteins are an essential part of signaling and transport processes and are targeted by multiple drugs. To isolate and investigate them in their native state, polymer-bounded nanodiscs have become valuable tools. In this study, we investigate the lipid model system dimyristoyl-phosphocholine (DMPC) with the nanodisc-forming copolymers styrene maleic acid (SMA) and diisobutylene maleic acid (DIBMA). Using small-angle X-ray scattering (SAXS) and dynamic light scattering (DLS), we studied the influence of polymer concentration and temperature on the nanodisc structure. In Tris buffer, the size of nanodiscs formed with SMA is smaller compared to DIBMA at the same polymer ratio. In both cases, the size decreases monotonically with increasing polymer concentration, and this effect is more pronounced when using SMA. Measurements at temperatures (T) between 5 and 30 °C in phosphate buffer showed an incomplete solubilization at high T even at polymer/lipid ratios above that required for complete lipid solubilization. For DIBMA, the nanodiscs developed at lower temperatures are stable and the net repulsion increases, while for SMA, the individual nanodiscs possess smaller sizes and are less affected by T. However, using DLS, one can observe SMA agglomerates at low T. Interestingly, for both polymers, no drastic changes of the observable parameters (radius and bilayer thickness) are seen upon cooling, which would indicate a sharp (first-order) phase transition from liquid-crystalline to gel, but only gradual changes. Hence, we conclude that the transition from a gel toward a liquid-crystalline lipid phase proceeds over a broad T-range compared to a continuous lipid bilayer. These results can pave the way toward the development of better protocols for studying membrane proteins stabilized in this type of membrane mimics.

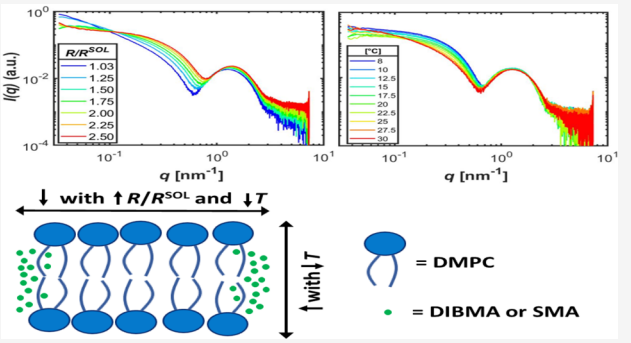

INTRODUCTION

Membrane proteins comprise approximately 26% of the human proteome.[1] They play essential roles in signaling and transport across cellular membranes and are the target of more than 60% of all drugs.[2] Frequently, membrane proteins must be extracted and purified for their study, which is commonly done using detergents. In general, detergents solubilize lipid bilayers into mixed micelles. Despite their efficiency as solubilizers, detergents provide an environment which poorly mimics that of a lipid bilayer, often resulting in low protein stability, loss of conformation, or aggregation.[3]

In 2002, so-called nanodiscs emerged as a solution to overcome these obstacles for membrane protein investigations.[4] For that, membrane-scaffolding proteins (MSPs) have been used as a belt to surround a lipid bilayer and stabilize it.[4,5] These lipid−protein particles were on the order of ≈ 10 nm in diameter, and due to their architecture as nanosized lipid bilayers they have been given the name nanodiscs.[4,6] Structural studies have been conducted to test different quantities. For example, Morgan et al. showed that the respective scaffolding protein is able to undergo structural changes.[6] Protein-nanodiscs have enabled biophysical and chemical investigations of several different membrane proteins including ion transporters and cytochrome P450.[7−10]

Using synthetic polymers as the surrounding belt instead of MSPs has enabled the fine-tuning of the size of the nanodiscs.[11] Another advantage of using a polymer as the belt compared to a MSP is the increased stability of the nanodiscs at low pH-values and in the presence of multivalent metal ions.[11] Also, no detergents are required for solubilization, which have to be removed in the end, and since no MSP is present, it cannot interfere with absorbance studies of the desired membrane protein.[12] The architecture of such polymer nanodiscs, i.e., the model used for fitting the experimental data, can be found in Figure 1a. Recently, the amphiphilic copolymers styrene maleic acid (SMA) (Figure 1b) and diisobutylene maleic acid (DIBMA) (Figure 1c) have been applied in the solubilization of model and natural lipid membranes.[13] In the presence of lipid membranes, these copolymers spontaneously form polymer-bounded lipid nanodiscs termed SMA-lipid particles (SMALPs)[14] or DIBMA-lipid

Received: December 20, 2022
Revised: January 24, 2023
Published: February 1, 2023

https://doi.org/10.1021/acs.langmuir.2c03412
Langmuir 2023, 39, 2450−2459

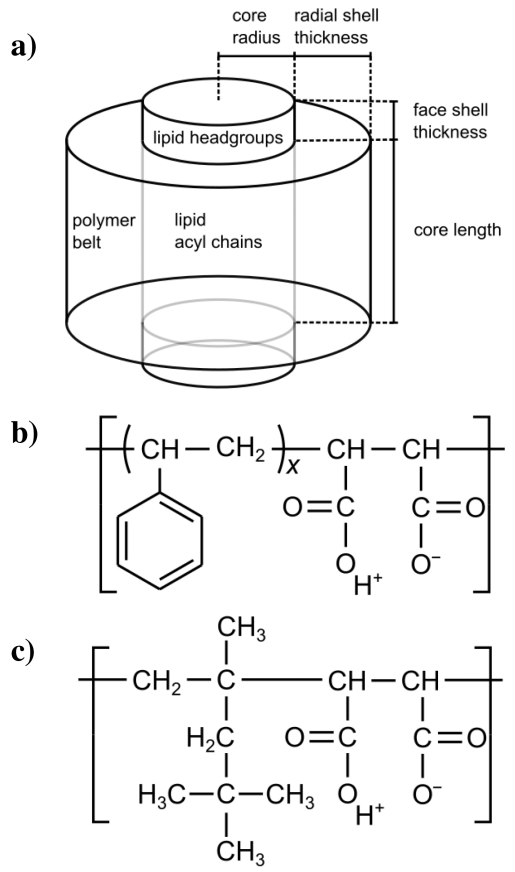

Figure 1. (a) Core−shell cylinder model used to fit SAXS data showing the dimensions calculated from the model. Chemical structures of (b) SMA(2:1) ($x \approx 2$, M_w = 7.0 kg/mol, M_n = 2.7 kg/mol) and (c) DIBMA (M_w = 15.3 kg/mol and M_n = 8.4 kg/mol).

particles (DIBMALPs), respectively.[15] These polymer nanodiscs can stabilize membrane proteins and are amenable to biophysical methods requiring small particle sizes in suspension and can allow the study of the membrane proteins with methods/techniques typical of soluble proteins.[16] Additionally, the lipid core of the nanodiscs can undergo gel-to-liquid thermotropic phase transitions, indicating the presence of a true lipid bilayer.[15,17−19]

Despite efforts to address the structural details of polymer nanodiscs,[12,15,20−23] little is known about the structural and molecular changes at different temperatures, i.e., how the (possible) phase transitions can affect the structure and polymer/lipid ratios. However, Bjørnestad et al. showed by small-angle X-ray scattering (SAXS) how solubilization from lipid vesicles proceeds upon polymer addition due to the self-insertion of styrene units into the lipid bilayer hydrocarbon (tail) region in a first step.[23] In the next step, upon increasing polymer (SMA(3:1), molar ratio of 3:1 styrene:maleic acid) concentration, the vesicle bilayers are saturated with polymer, and SMA nanodiscs begin to form as the polymer molecules form a belt around the structure.[23] In this stage, the nanodiscs coexist with the polymer-saturated lipid vesicles.[23] In the last step, upon crossing the solubilization polymer concentration, all lipid vesicles are fully transformed into SMA nanodiscs.[23] Similar observations were obtained by molecular dynamics simulations. There, SMA was found to bind to the lipid bilayer interface, which is caused by the hydrophobic effect.[24] Increasing the amount of adsorbed polymer leads to large membrane defects, including small, water-filled pores.[24] The rim of these pores can be stabilized by the SMA molecules, resulting in pore growth and further membrane disruption.[24] In their simulations, no complete nanodisc formation was seen due to the limited time scale of the simulations.[24] However, self-assembly simulations indicate that nanodiscs are the thermodynamically most favorable state of these systems.[24]

In the present work, we have exploited SAXS and dynamic light scattering (DLS) to systematically investigate the structural changes of polymer nanodiscs formed with the saturated phospholipid dimyristoylphosphocholine (DMPC) and either SMA(2:1) (2:1 styrene:maleic acid) or DIBMA (1:1 diisobutylene:maleic acid). Taking advantage of published pseudophase diagrams,[15,18] we produced SMALPs and DIBMALPs at copolymer/lipid molar ratios (R) above that required to achieve complete lipid solubilization (R^{SOL}) and analyzed changes in their geometry and molecular arrangement at increasing R (case A) and temperature of the system (case B). For SMALPs, R^{SOL} is 0.13 and for DIBMALPs 0.062 for the lipid concentration used in this work.[15,18] We found that the average diameter d of the polymer nanodiscs decreases monotonically with increasing R and that d(SMA) < d(DIBMA) at the same R/R^{SOL} values. In contrast, the bilayer thickness is only reduced significantly for SMALPs but to a much smaller extent for DIBMALPs. For case B, a decrease in the system temperature results in a contraction of the diameter and concomitant increment of the nanodisc thickness in both SMALPs and DIBMALPs. Decreasing the temperature leads to a complete solubilization and complete nanodisc formation for both polymers.

EXPERIMENTAL SECTION

Materials. 1,2-Dimyristoyl-*sn*-glycero-3-phosphocholine (DMPC) was from Avanti (Alabaster, AL). Solutions of styrene/maleic acid 2:1 (SMA(2:1)) (trade name Xiran SZ30010) and diisobutylene/maleic acid (DIBMA) (trade name Sokalan CP9) were kindly provided by Polyscope (Geleen, Netherlands) and BASF (Ludwigshafen, Germany), respectively. NaCl, Na_2HPO_4, NaH_2PO_4, and tris(hydromethyl)aminomethane (Tris) were purchased from Sigma−Aldrich (Steinheim, Germany). All chemicals were purchased at the highest purity available.

Polymer Stock Preparation. SMA(2:1) hydrolyzed from styrene maleic anhydride (2:1) (mass-average molar mass M_w = 7.0 kg mol^{-1} and number-average molar mass M_n = 2.7 kg mol^{-1}) and DIBMA (M_w = 15.3 kg mol^{-1} and M_n = 8.4 kg mol^{-1}) were obtained as alkaline solutions. The copolymers were prepared as described previously.[25] Briefly, the copolymer in solution was precipitated by adding small amounts of concentrated HCl and gently shaking until the solution reached pH ≈ 5. The suspension was centrifuged at 11 000g at room temperature (RT) for 15 min and the supernatant discarded. The copolymer was resuspended in 100 mL of ultrapure water by vigorous shaking and centrifuged at 11 000g at RT. The copolymer was resuspended in ultrapure water and centrifuged twice again. Precipitated copolymer was resuspended in 0.5 M NaOH at 37 °C under gentle shaking. After complete resuspension, the copolymer was frozen at −80 °C and freeze-dried for at least 24 h. Dried copolymer powder was stored in a dark sealed glass container at RT and resuspended in buffer before use.

Preparation of Polymer−Lipid Nanodiscs. DMPC in the form of dried lipid powder was resuspended in Tris−saline (TS) buffer (50 mM Tris, 200 mM NaCl, pH 7.4) or phosphate−saline (PS) buffer (50 mM Na_2HPO_4/NaH_2PO_4, 200 mM NaCl, pH 7.4) to a final concentration of 20 mM. The lipid suspension was thoroughly vortexed and equilibrated at 30 °C for 15 min prior to a 31-fold extrusion through a 100 nm polycarbonate membrane using a LiposoFast extruder (Avestin, Ottawa, Canada) to form large

https://doi.org/10.1021/acs.langmuir.2c03412
Langmuir 2023, 39, 2450−2459

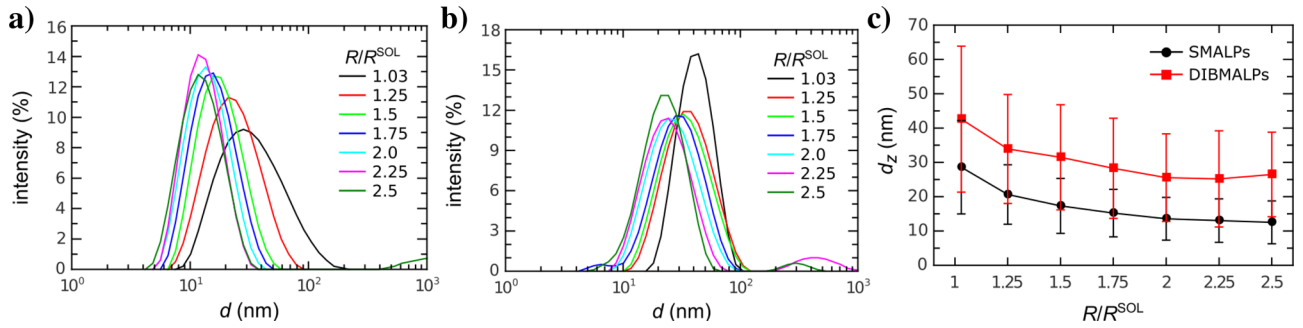

Figure 2. Size of SMALPs and DIBMALPs as monitored by DLS at 30 °C. Intensity-weighted particle size distributions as a function of hydrodynamic diameter, d, for (a) SMALPS and (b) DIBMALPs. Legend indicates the normalized polymer/lipid ratio of nanodisc formation with the corresponding solubilizing polymer/lipid ratio (R/R^{SOL}). (c) z-average particle size, d_z, as obtained from curves in (a) and (b). Error bars indicate the peak distribution width as determined from $\sigma = d_z\sqrt{\text{PDI}}$. Nanodiscs were formulated in TS buffer.

unilamellar vesicles (LUVs). LUVs were mixed and incubated with either SMA(2:1) or DIBMA in TS buffer for concentration-dependent experiments or in PS buffer for temperature-dependent experiments at 30 °C for at least 1 h to form SMALPs or DIBMALPs, respectively. The reason we used phosphate buffer for temperature-dependent experiments is that Tris buffer undergoes pH changes at different temperatures and, thus, can affect nanodisc shape/formation.[26] SMALPs and DIBMALPs were always produced with a final lipid concentration of 10 mM and a R above that required for complete lipid solubilization (R^{SOL}).[18,19]

SAXS Measurements. SAXS measurements were performed at P12, PETRA III at DESY, Hamburg, Germany.[27] The data were reduced according to standard procedures using the beamline software and scaled to absolute scattering intensity, $I(q)$, with units of 1/cm as a function of q with $q = 4\pi\sin\theta/\lambda$ where θ is half the scattering angle and λ the wavelength of the incoming bean. The incident beam had an energy of 10 keV. Calibration of the intensity was made using bovine serum albumin as a protein standard or ultrapure water.

SAXS Data Analysis. SAXS data were analyzed in both a model-free and a model-dependent way in order to obtain as much information as possible. For the model-free approach, the pair density distribution function (PDDF, $P(r)$) and the radius of gyration R_g of the respective SAXS curves were calculated by GNOM (Version 4.6).[28] An effective bilayer thickness could be obtained by the position of the second maximum in each curve representing the correlation between the headgroups. After having confirmed that the shape of the particles can be indeed assumed as flat discs, a poly core−shell cylinder model was applied to fit the SAXS curves using IGOR Pro 6.37 in combination with the NIST analysis package.[29] The scattering length density (SLD) of the core, i.e., the hydrophobic tails of the lipids, was calculated to be 4.7×10^{-8} Å^{-2} and set constant. The SLD of the shell (taking into account the polymer belt as well as the hydrophilic headgroups of the lipids) was set to $\approx 8 \times 10^{-8}$ Å^{-2}. All other parameters were left free for fitting. The bilayer thickness, t, was subsequently calculated as 2 × face shell thickness + core length, whereas the diameter of the nanodiscs, d, was calculated by 2 × core radius + 2 × radial shell thickness.

DLS. DLS measurements were performed on a Zetasizer Nano ZS (Malvern Instruments, Worcestershire, U.K.) equipped with a 633 nm He−Ne laser and a photodetector placed at an angle of 173°. Measurements were carried out in a quartz cuvette with a 3 × 3 mm cross section (ZEN2112, Malvern Instruments). Samples were measured with the attenuator position automatically optimized for determination of size distributions. Data analysis was performed by fitting the experimentally determined autocorrelation function with a non-negative constrained least-squares function[30] to obtain the intensity-weighted particle size distribution and by cumulant analysis[30] to yield the z-average particle size and size distribution width as derived from the associated polydispersity index (PDI). Assuming Gaussians distributions of both the decay rate and the particle size, the standard deviation of the z-average particle size was determined as $\sigma = d_z\sqrt{\text{PDI}}$.

RESULTS AND DISCUSSION

Case A: Membrane Architecture Is Affected by Increasing Copolymer Concentrations. To test the influence of copolymer type on nanodisc formation, we produced SMALPs and DIBMALPs by solubilizing large unilamellar vesicles (LUVs) made up of DMPC. Both polymers are similar except the fact that SMA contains a styrene residue whereas DIBMA's residue is aliphatic (see Figure 1b and c). It has been reported that combining lipids with SMA or DIBMA at subsolubilizing polymer/lipid ratios below R^{SOL} leads to incomplete vesicle solubilization and subsequent formation of large aggregates which are incompatible with methods requiring small particle sizes.[31] Thus, we produced SMALPs and DIBMALPs at R greater than R^{SOL}.[18,19,32] SMALPs and DIBMALPs produced with increasing R were first analyzed by DLS to determine their mean hydrodynamic size (z-average) and polydispersity.[33] The z-average sizes of the SMALPs ranged from 13 ± 6 up to 29 ± 14 nm (Figure 2a) and of the DIBMALPs from 26 ± 12 up to 43 ± 21 nm (Figure 2b). Notably, the polydispersity of both systems remained consistently low at all R, as reflected in the relatively narrow peak widths derived for each particle population. The DLS results confirm the dependence of particle size on copolymer/lipid ratio of formation and the ability of DIBMA to form larger nanoparticles as compared with SMA. This information can be relevant for exploiting DIBMA's potential to directly extract large molecular complexes from biological membranes or to use it as a platform for membrane protein reconstitution.

Although DLS is a valuable method for gaining information about globular particle sizes, it is not able to resolve smaller-scale characteristics of the particles of interest.[34] Hence, we used SAXS to obtain detailed information on the size and structure of nanodiscs in solution. The recorded SAXS data show an oscillating behavior of the scattering intensity arising from negative excess scattering length density from the hydrocarbon chains at the nanodisc core and positive excess length densities from both the phosphocholine headgroups and the copolymer belt on both SMALPs and DIBMALPs (Figure 3).[23,35−37] The SAXS pattern is similar to that of structurally similar particles such as lipoprotein−lipid complexes[38] and protein-bounded nanodiscs,[39,40] evidencing the discoidal shape of SMALPs and DIBMALPs. The data for SMALPs show a

https://doi.org/10.1021/acs.langmuir.2c03412
Langmuir 2023, 39, 2450−2459

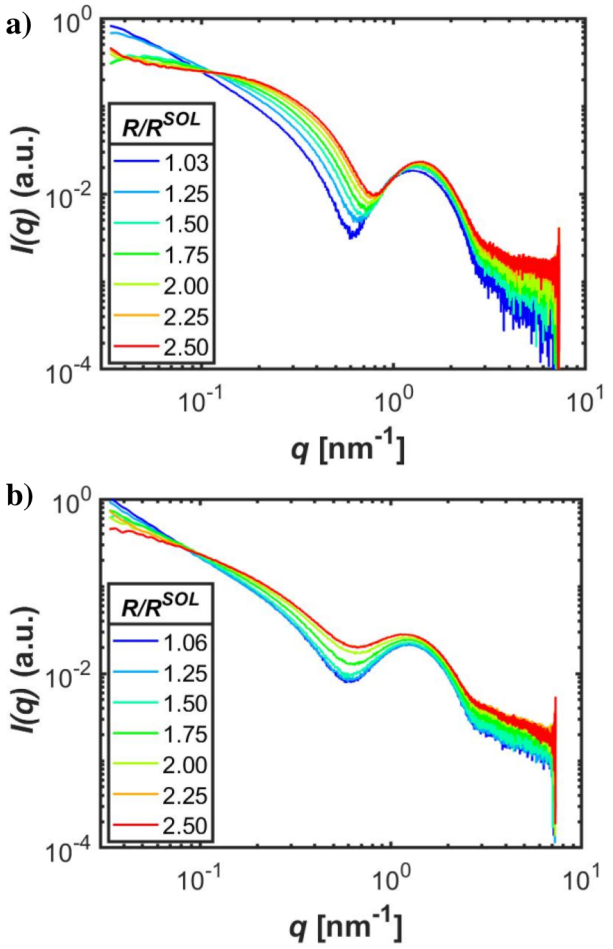

Figure 3. SAXS scans for (a) SMALPs and (b) DIBMALPs produced at increasing copolymer/lipid ratio, measured at 30 °C. Nanodiscs were formulated in TS buffer.

local minimum at the scattering vector q = 0.6 nm^{-1}, which shifts to higher q-values accompanied by a reduction in its depth with increasing SMA concentrations (Figure 3a). A shift of the minimum from q = 0.6 nm^{-1} to q = 0.8 nm^{-1} represents a decrease in the nanodisc radius from $d = 2\pi/q_{min} = 2\pi/0.6$ nm^{-1} = 12.4 nm to $d = 2\pi/0.8$ nm^{-1} = 7.8 nm. Conversely, DIBMALPs only present a marginal shift of the local minimum at q = 0.6 nm^{-1} but a noticeable reduction of its depth with increasing copolymer fractions (Figure 3b). The shift of the minimum to higher q-values indicates a decrease in size of the particles with increasing R/R^{SOL} ratio, which seems to be more pronounced for SMALPs. In addition, both systems change their behavior similarly at low q-values. There, the slope of the SAXS curves decreases and becomes more and more flat, indicating that the molecular weight for the individual nanodiscs decreases with increasing R, being consistent with a reduction of their size.

Real-space representations of the SAXS data in the form of pair density distribution functions were determined via indirect Fourier transform (Figure 4a and b).[41] All curves display a similar shape at low r-values, indicating similar distribution densities for all nanodiscs: a minimum flanked by two local maxima which are followed by a long tail at about 12 nm. The shape of these curves is typical for lipid bilayers,[42] which have negative scattering contrast at the central part of the particle and a positive one at the edges. Since X-rays scatter at the electrons of the atoms, the scattering contrast refers to the difference in electron density between the particles investigated and the respective solvent of the system, and only the difference between these two electron densities is detectable. The local maximum at 5.5−6.5 nm is of particular importance as is determined by the lipid bilayer thickness (Figure 4c), which corresponds to the sum of the core length and two times the lipid headgroups represented by the face shell thickness (Figure 1a). It decreases steadily from 6.5 to 5.3 nm for SMALPS, while the thickness of the DIBMALPs seems to be unaffected upon increasing the polymer/lipid ratio on the particles. Since the r-value at which the pair density distribution function declines to zero again indicates the maximum dimensions within the particle, the tail at high r-values is most likely emerging from copolymer chains protruding from the nanodisc. Since it decays to zero at much lower R/R^{SOL} for SMALPs than for DIBMALPs, we assume that the SMA molecules interact more strongly with the bilayer core due to their styrene residue and do not protrude as much as the DIBMA molecules do. This is also supported by the bilayer thickness decrease of the SMALPs but not of the DIBMALPs (Figure 4c). Due to the strong interactions with the hydrocarbon chains of the nanodiscs, potentially their effective length and therefore the bilayer thickness could be reduced.

Furthermore, we calculated the radius of gyration (R_g), corresponding to the radial distance of the nanodiscs to their center of mass (or, equivalently, the diameter (d, expressed as $2 \times R_g$). These parameters are more affected by the copolymer molar fraction on SMALPs as compared to DIBMALPs (Figure 4d). These results are in agreement with the DLS and raw SAXS data which generally show a decreasing size with increasing polymer concentration for both systems.

Taken together, these results indicate that the generally smaller SMALPs undergo a reduction of both the nanodisc diameter and the bilayer thickness populating the core with increasing polymer/lipid ratios. In contrast, the average DIBMALP diameter is less affected by an increment of the DIBMA ratio, whereas the bilayer thickness remains virtually unaffected. However, a detailed nanodisc structure is far too complex to allow for a model-free interpretation based on only the inspection of the SAXS and DLS data.

To gain further insights, we analyzed the SAXS data using a core−shell cylinder model (Figure 1a). The fit results (Figure S1, Table S1) show that for both SMALPs and DIBMALPs, the radius of the nanodisc core is quickly reduced upon increasing the polymer/lipid ratio (Figure 5a and b). In SMALPs, it decreases from ≈ 9 nm at R/R^{SOL} = 1.03 and seemingly saturates at ≈ 3 nm, whereas DIBMALPs are bigger with a core radius of ≈ 13 nm at low R and ≈ 6 nm at R/R^{SOL} = 2.5. Conversely, the nanodisc thickness increases slightly from ≈ 4 to ≈ 5 nm for SMALPs but is apparently unaffected for DIBMALPs. To split the different contributions of each component and gain further insight, we analyzed the core length and face shell thickness (see Figure 1a). For SMALPs, the core length decreases with increasing polymer concentration while the face shell thickness increases. On the other hand, for DIBMALPs, the core length increases while the face shell thickness decreases. In the latter case, the moduli of these two changes are similar, compensating each other. Thus, in total, the bilayer thickness does not change. As already mentioned above, this behavior is consistent with the literature, which states less perturbation of the DMPC

https://doi.org/10.1021/acs.langmuir.2c03412
Langmuir 2023, 39, 2450−2459

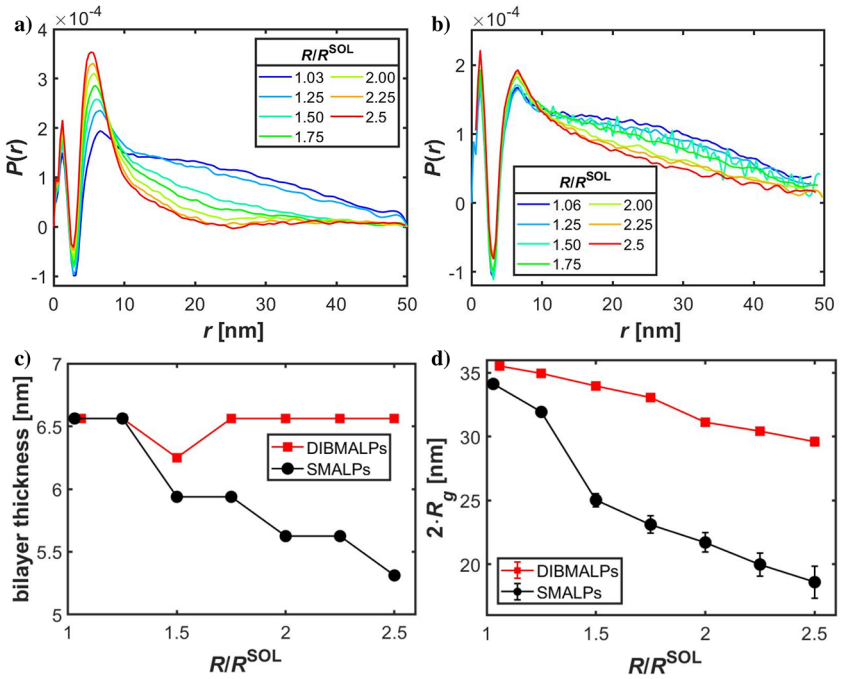

Figure 4. Pair density distribution functions, $P(r)$, of (a) SMALPs and (b) DIBMALPs determined from SAXS scans presented in Figure 3a and b, respectively. (c) Bilayer thickness as a function of R/R^{SOL} and (d) nanodisc size, expressed in terms of radii of gyration, R_g. Nanodiscs were formulated in TS buffer. The error bars, if not visible, are smaller than the symbols.

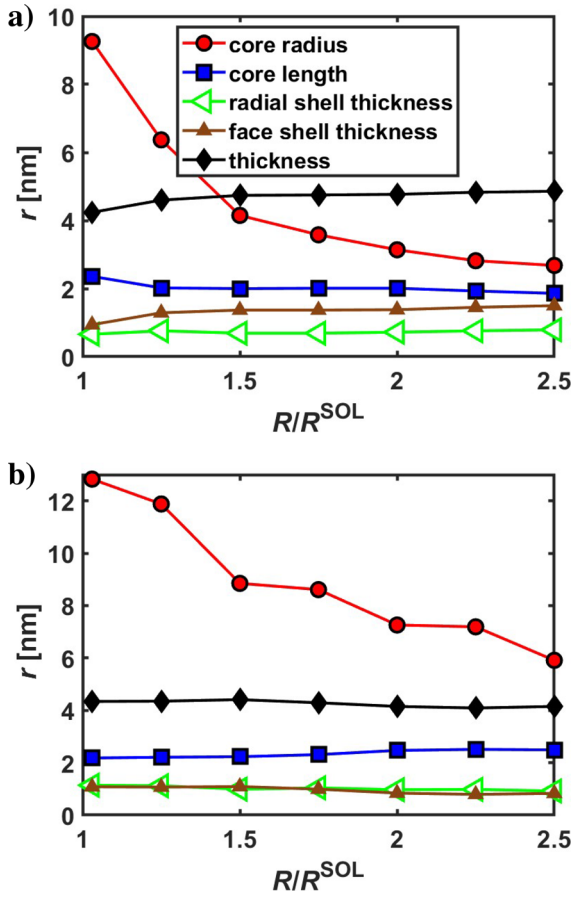

Figure 5. Fit parameters calculated for (a) SMALPs and (b) DIBMALPs from SAXS data fit to the model (Figure 1a). Fitted values are detailed in Table S1 and the corresponding fits in Figure S1. Nanodiscs were formulated in TS buffer.

phospholipids populating the nanodisc core compared to SMA.[15,18] Similar to the model-free analysis (Figure 4d), a larger radius for the DIBMALPs than for the SMALPs is obtained and the respective radius decreases with increasing polymer concentration (Figure 5b). The thickness of the SMALPs increases in the core−shell cylinder model (Figure 5a), whereas it decreases in the model-free analysis (Figure 4c). This can be explained by the fact that the pair density distribution function takes into account the most probable or frequent distance between the lipid headgroups, whereas the model assumes an average or mean for the same distance. Furthermore, a distinction between the scattering signal contribution of different parts of the nanodiscs is extremely difficult. This is the case because a decrease in the core length is visible for SMALPs, but the lipid headgroups do not change their size and therefore may also be surrounded by polymer (see Figure 1a). We note that, similar to a recent study, we observe a rather constant thick polymer belt (here: radial shell thickness, see Figure 1a).[23] Therefore, we also conclude that the number of SMA particles within the belt decreases with decreasing radius as the excess copolymer distributes mainly in the belt structure after solubilization.[23]

Case B: Influence of Temperature on the Size and Shape of Nanodiscs. To study the influence of temperature and check for possible phase transitions of the lipid within the nanodiscs, SMALPs and DIBMALPs produced at R/R^{SOL} = 1.25 were analyzed using DLS and SAXS between 30 and 5 °C, that is, above and well below the melting temperature (T_m) of DMPC bilayers (24 °C).[12,19] Note that for the temperature measurements PS instead of TS buffer was used to minimize pH effects upon quenching.[26]

DLS analysis on SMALPs and DIBMALPs produced at R/R^{SOL} = 1.25 shows a reduction in the z-average mean size of both types of nanoparticles with decreasing temperature (Figure 6a−c). However, we shall discuss the effect of

https://doi.org/10.1021/acs.langmuir.2c03412
Langmuir 2023, 39, 2450−2459

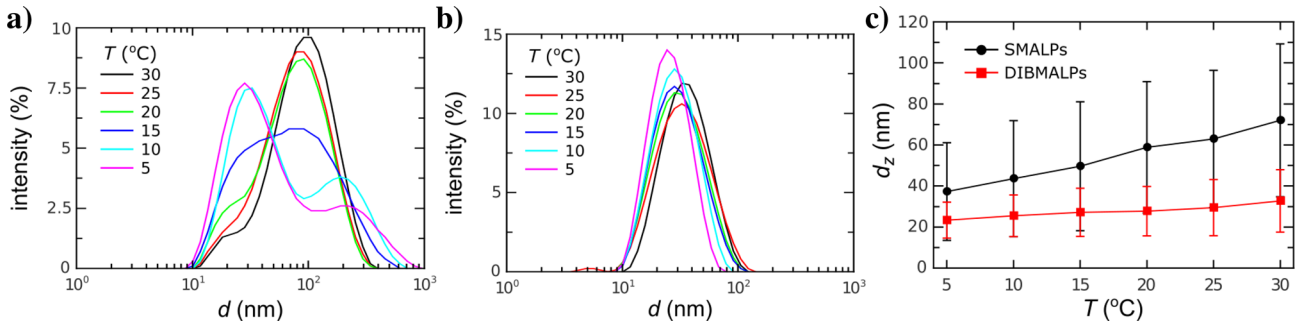

Figure 6. SMALP and DIBMALP sizes as monitored by DLS at decreasing temperatures. Intensity-weighted particle size distributions as a function of hydrodynamic diameter, d, for (a) SMALPs and (b) DIBMALPs measured between 5 and 30 °C. (c) z-average particle diameter, d_z, as calculated from curves in (a) and (b). Vertical bars indicate peak widths derived from the corresponding polydispersity values. Nanodiscs were formulated at R/R^{SOL} = 1.25 in PS buffer.

exchanging the buffer. First, SMALPs are the larger species in PS buffer, whereas DIBMALPs are larger in TS buffer at this polymer/lipid ratio (Figures 2c and 6c). Additionally, SMALPs show a clear bimodal size distribution in PS, especially at lower temperatures (Figure 6a). The peak for the larger particles is roughly at 100 nm and shifts toward larger sizes, whereas the smaller particles consist dominantly of sizes between 20 and 30 nm. Upon temperature quenching down to 5 °C, the peak for the larger length/diameter (≈ 200 nm) decreases in height, and the smaller peak (≈ 30 nm) becomes dominant. We conclude that initially, at 30 °C, large aggregates/clusters of nanodiscs and/or an incomplete solubilization of the LUVs is still present. The signal corresponding to undissolved vesicles might arise from hemifused nanodiscs, since these were formulated at a R/R^{SOL} ratio just above the solubilization threshold for this set of experiments. Upon quenching, single/separated nanodiscs emerge (indicated by the 20 nm peak) as well as clusters/aggregates of the nanodiscs (as indicated by the 200 nm peak). For DIBMALPs, the effect of temperature (and solvent) seems weaker (Figure 6b and c). Nevertheless, the nanodiscs are smaller in size in PS buffer, and a decrease of the intensity-weighted particle size (and distribution) is found. Hence, we speculate that the phosphate buffer in particular hinders the styrene group of SMA to interact not only with the lipid core (at elevated temperatures) but also with other nanodiscs/polymers to prevent aggregation at lower temperatures.

SAXS curves arising from SMALPs show a steady increment of the signal intensity at low q-values with decreasing temperatures (Figure 7a). As stated above, this indicates a transition toward a system with particles having a higher molecular weight. This is consistent with the shift of the larger particle peak seen by DLS toward larger sizes (see Figure 6a). This effect dominates the scattering signal at low q-values, and an increase in the amount of solubilized nanodiscs cannot be observed in contrast with the DLS data (see Figure 6a). However, the minimum at q = 0.6 nm^{-1} shifts slightly toward higher q-values upon quenching, indicating the reduction of the nanodisc sizes, which is also consistent with DLS data showing the formation of single and separated nanodiscs. SAXS scattering curves arising from DIBMALPs exhibit a different behavior at low and intermediate q-values (< 0.6 nm^{-1}) with decreasing temperatures (Figure 7b). We note that the raw SAXS data of DIBMALPs suggest an incomplete solubilization at higher temperatures,[23] whereas quenching leads to a more complete solubilization and formation of nanodiscs (Figures 7b and 8b). This is supported by the shift

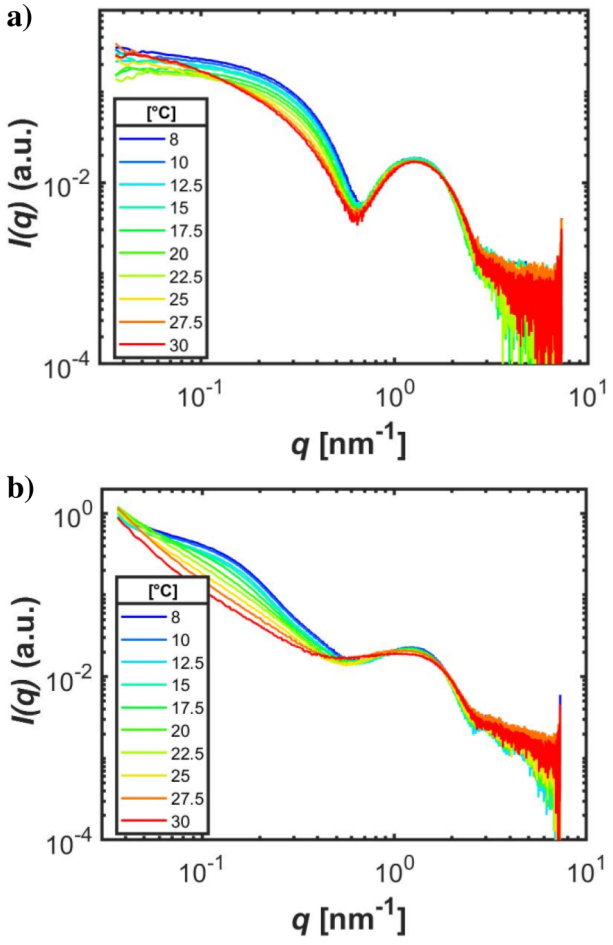

Figure 7. SAXS scans for (a) SMALPs and (b) DIBMALPs measured between 8 and 30 °C. Nanodiscs were formulated at R/R^{SOL} = 1.25 in PS buffer.

of the minimum toward higher q-values and therefore smaller particles in solution. Similar observations have been made for lipid vesicles in the presence of polymer concentrations below the solubility limit R^{SOL}.[23] The straight line at 30 °C transforms into a shoulder at roughly q = 0.1 nm^{-1}, corresponding to a real-space distance ($r = 2\pi/q$) of $r \approx 60$ nm. It becomes more pronounced with decreasing temperature and mirrors the maximum size/length of the nanodiscs: from large, polydisperse particles at 30 °C, the system transforms into smaller, more monodisperse particles with a length of

https://doi.org/10.1021/acs.langmuir.2c03412
Langmuir 2023, 39, 2450−2459

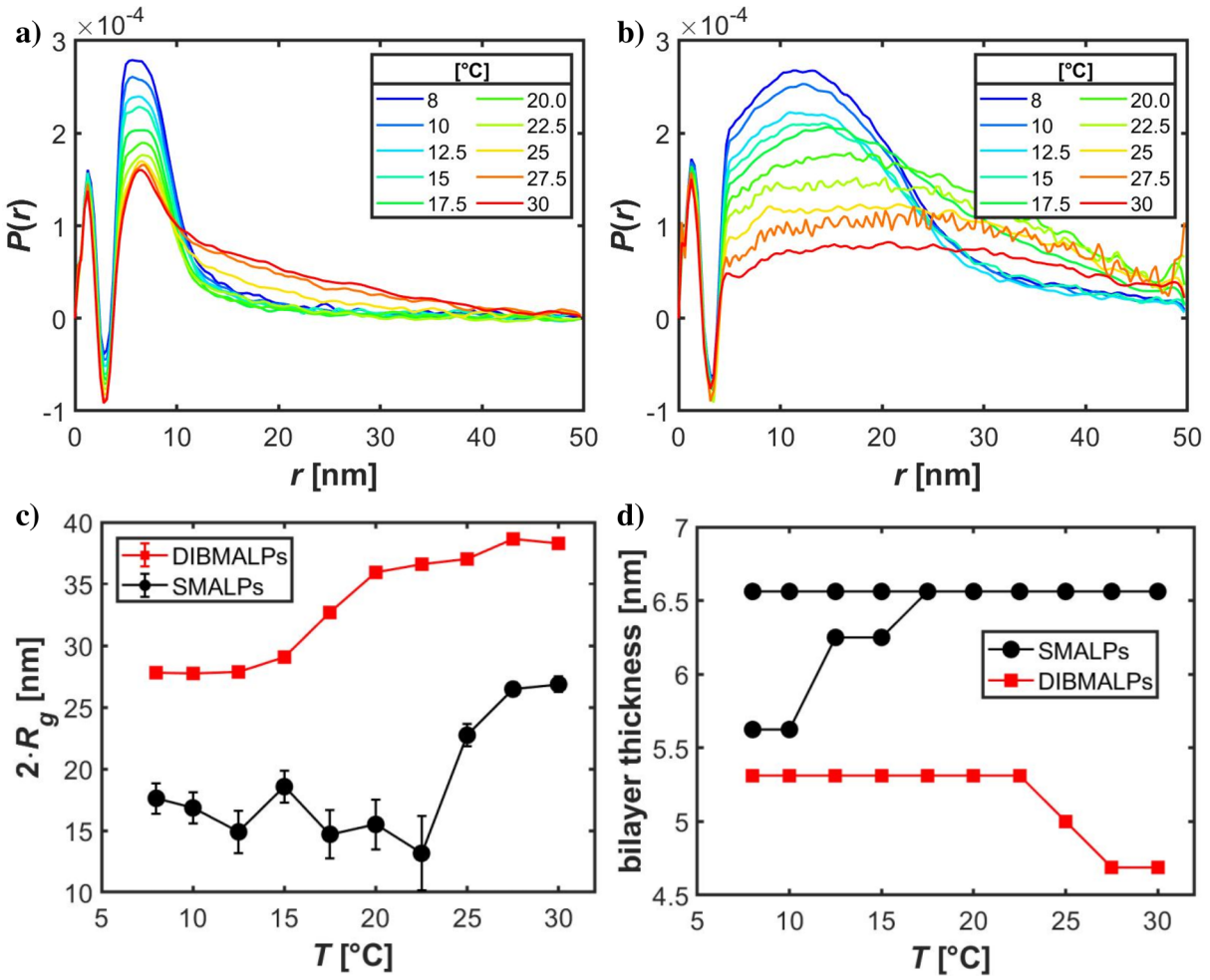

Figure 8. Calculated pair density distribution functions, $P(r)$, of (a) SMALPs and (b) DIBMALPs at increasing temperatures as derived from SAXS curves in Figure 7a and b, respectively. (c) Particle radii of gyration, R_g (expressed as $2R_g$), and (d) bilayer thickness of SMALPs and DIBMAPs as a function of temperature. Nanodiscs were formulated at R/R^{SOL} = 1.25 in PS buffer. The error bars, if not visible, are smaller than the symbols.

roughly 60 nm upon quenching (see also DLS data (Figure 6b and c)). Hence, the scattering curves reflect the interparticle correlation; at high temperatures, an effective attraction resulting in a melt or an extended polymer chain entanglement is present. In contrast, at low temperatures, this entanglement dissolves into single/separated nanodiscs because of a net repulsion within the system. Thus, the raw data at high temperatures as well as the corresponding PDDFs do not exhibit the behavior expected for nanodiscs and are therefore difficult to analyze. At R/R^{SOL} = 1.25, we would assume that the formation of nanodiscs is complete, but the different buffer used for the temperature measurements (PS vs TS) appears to play a role. The calculated PDDFs indicate a strong temperature-dependent effect on the nanodisc morphology. At 30 °C, the SMALPs exhibit a single peak at $r \approx 7$ nm, which broadens and evolves into two peaks upon temperature reduction (Figure 8a). As a result, the DMPC bilayer thickness determined for SMALPs is 6.5 nm at 30 °C and transitions toward two distinctive bilayer thicknesses with decreasing temperature (Figure 8d). Additionally, the long tail at high r-values decreases and vanishes at lower r-values with decreasing temperature, indicating a reduction in size (Figure 8a), consistent with DLS and SAXS data. DIBMALPs present a more complex pattern; at 30 °C, the small peak at ≈ 4.7 nm has nearly disappeared, and a broad peak with a local maximum at $r \approx 13$ nm appears at lower temperatures (Figure 8b). Since a complete solubilization of the lipid vesicles occurs only for lower temperatures (< 20 °C), it is impossible to determine the maximum of the PDDF curves as before. Nevertheless, for further quenching and, hence, finalizing solubilization, the bilayer thickness of DIBMALPs remains constant at 5.3 nm. The calculated R_g for SMALPs indicates particles with an average diameter of ≈ 25 nm at 30 °C, which decreases quickly upon temperature reduction to ≈ 15 nm (Figure 8c), whereas DIBMALPs' average diameter was 38 nm at 30 °C and was reduced in a more stepped manner until reaching 27 nm (Figure 8c).

Using the core−shell cylinder model, we observe first an increase of the core radius of SMALPs upon quenching, until a gradual decrease is observed (Figure 9). During the quenching process, the bilayer thickness increases slightly, suggesting a liquid-crystalline to gel phase transition. This increase in bilayer thickness is even visible for DIBMALPs in the reasonable low-temperature regime, where a complete solubilization took place (Figure 9). The following parameters are essentially unchanged and, thus, are not plotted for clarity but are mentioned in the following. For SMALPs, the core length is in a range between 1.2 and 1.4 nm, the radial shell thickness between 0.6 and 1 nm, and the face shell thickness is 2.1 nm. In contrast, for DIBMALPs, the core length is in the

https://doi.org/10.1021/acs.langmuir.2c03412
Langmuir 2023, 39, 2450−2459

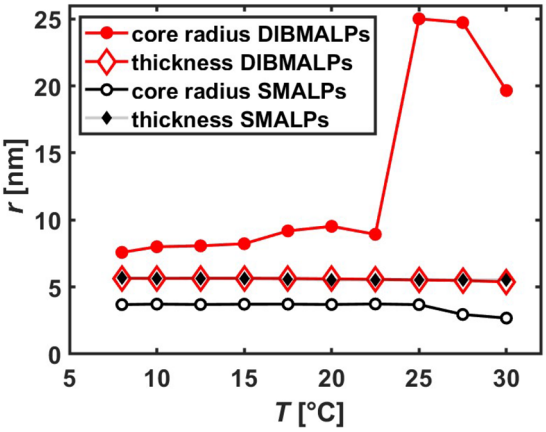

Figure 9. Selected fit parameters calculated for SMALPs (black) and DIBMALPs (red) obtained from SAXS data fit to the core−shell cylinder model (Figure 1a). All fit parameters can be found in Table S2, and the corresponding fits are shown in Figure S2. Nanodiscs were formulated at R/R^{SOL} = 1.25 in PS buffer.

interval 0.7−0.8 nm, the radial shell thickness between 1.9 and 3 nm (decreasing with decreasing T), and the face shell thickness is 2.4 nm. As the radial shell thickness of the SMALPs decreases with decreasing T, we speculate that more SMA molecules are transferred from the polymer belt toward the interior of the nanodiscs due to quenching.

Discussion. Taken together, these results indicate that SMALPs and DIBMALPs undergo a reduction in the average diameter with decreasing temperatures and that the buffer used plays a non-negligible role. In PS buffer, SMALPs are 2−3 times larger than DIBMALPs in the temperature range investigated. Due to the buffer exchange, both systems seem to display incomplete solubilisation at 30 °C. For DIBMALPs, solubilization seems to improve upon quenching, whereas SMALPs can aggregate at lower temperatures. Moreover, the DMPC bilayers most likely transition from the liquid-crystalline to gel phase below 24 °C. SANS studies performed on DMPC bilayers have shown that lipids in the gel phase occupy less area per molecule as compared with fluid phase lipids and have increased hydrocarbon thickness.[43,44] This leads to closer lipid packing and can account for the reduction in the average nanodisc diameter with concomitant increment in the bilayer thickness. Additionally, EPR studies on SMA-stabilized nanodiscs have shown that the copolymer styrene groups strongly interact with the phospholipids' acyl chains.[45,46] We speculate that, at low temperatures, the two membrane thicknesses observed in SMALPs can be a result of phase separation of the gel and liquid-crystalline phase lipids coexisting within individual nanodiscs as a result of strong local SMA−DMPC interactions at the nanodisc rim. Due to these strong interactions and additional incorporation of SMA into the nanodisc core, the thickness could be effectively decreased as the SMA molecules occupy positions of lipids. This can be a result of the polymer interacting dominantly with the nanodisc core (i.e., the hydrophobic part). Hence, as the SMA molecules are located there, some of the lipids (and therefore also their headgroups) are displaced and are absent compared to the nanodiscs formed at higher T, which may lead to the two thicknesses observed (Figure 8d). Note that already in case A, an increase in SMA concentration led to a decrease in the bilayer thickness of the nanodiscs (see Figure 4c), supporting this hypothesis.

We note that neither in the raw data nor in the analysis was a jump of the respective parameters seen, but but the changes were always continuous. We assume that the phase transition of the lipid within the nanodiscs is therefore not as sharp as for the pure lipid itself, but the phase transition temperature is rather smeared out. Already in 2012, a noncooperative thermotropic phase transition was reported for nanodiscs consisting of DMPC and SMA.[47] The authors attributed this to the smaller size of the nanodiscs compared to the pure DMPC vesicles and the presence of lipids that probably do not participate in the cooperative phase transition due to their interactions with the polymer and therefore their increased ordering compared with DMPC vesicles.[47,48] Similar to Bjørnestad et al., who recently reported that gel-like membranes more easily solubilize with SMA(3:1), we observe a seemingly more efficient solubilization at low temperatures.[23] This is not only true for SMA(2:1) but also for DIBMA. However, we assume a further aggregation of the SMALPs at low temperatures, leading to a species of particles with a size of 200 nm in addition to the separated and solubilized nanodiscs.

Noteworthy, different models for the analysis of small-angle scattering data of nanodiscs have been applied in the past. While Bjørnestad et al. applied an ellipsoidal core−shell mixed micelle model, a mixed lipid:SMA disc model, a lipid disc with a SMA belt model, and a mixed lipid:SMA disc with a SMA belt model to fit the data, with the latter one having the best results, Skar-Gislinge et al. developed a completely new model themselves.[35,36] Since the nanodiscs used by Skar-Gislinge et al. consisted of lipids and MSPs, they constructed their model with two histidine-tags protruding out from the belt, the MSP as the belt, and two caps from the lipid headgroups.[35] In addition, they separated the hydrophobic interior into a central low-density methyl group region, sandwiched between two higher density leaflets composed of the $(CH_2)_n$ chains.[35] To catch the important parameters but keep the model as simple as possible, we decided to use the core−shell cylinder model as it was proven before that the nanodiscs exhibit a disc-like architecture and the model fits the experimental data well.[23,35]

CONCLUSION

In summary, we have investigated the structure of membrane-mimicking nanodiscs composed of the lipid DMPC with two different polymers, SMA(2:1) and DIBMA, by SAXS and DLS. In a first approach, the polymer/lipid ratio was increased continuously (in TS buffer), starting from ratios above that required for complete lipid vesicle solubilization ($R/R^{SOL} \approx 1$) up to a ratio of R/R^{SOL} = 2.5. Here, DIBMALPs are larger for the same R/R^{SOL} ratios. The nanodisc radii formed by both polymers decrease with increasing R. This effect is more pronounced when using SMA, suggesting a stronger interaction of SMA with DMPC. In a second approach, temperature-dependent measurements between 5 and 30 °C were performed to study the effect of temperature on the architecture as well as on the (possible) phase transitions. For this purpose, PS buffer was chosen to avoid the influence of temperature-dependent pH changes. Nevertheless, this buffer exchange seems to have crucial effects. First, in PS buffer, SMALPs are the larger species at the polymer/lipid ratio used. Second, the lipid vesicles are not completely solubilized, even at R/R^{SOL} = 1.25 at 30 °C. Quenching leads in both cases to a complete solubilization and nanodisc formation. In this regard, DIBMALPs are stable at low T due to an increase in net repulsion. In contrast, nanodiscs formed with SMA aggregate

https://doi.org/10.1021/acs.langmuir.2c03412
Langmuir 2023, 39, 2450−2459

further at low T due to an increase in attraction. Interestingly, no sudden changes can be observed, which would indicate the presence of a sharp phase transition temperature. All changes are gradual and mirror a broad melting temperature range. These results are not only relevant from a fundamental point of view but also have an impact on the structural biology of proteins and potentially many other fields such as biopharmaceutical formulation.

■ ASSOCIATED CONTENT

Supporting Information

The Supporting Information is available free of charge at https://pubs.acs.org/doi/10.1021/acs.langmuir.2c03412.

Experimental SAXS data and corresponding fits as well as all fit parameters (PDF)

■ AUTHOR INFORMATION

Corresponding Author

Fajun Zhang − *Institut für Angewandte Physik, Universität Tübingen, 72076 Tübingen, Germany;* orcid.org/0000-0001-7639-8594; Email: fajun.zhang@uni-tuebingen.de

Authors

Ralph Maier − *Institut für Angewandte Physik, Universität Tübingen, 72076 Tübingen, Germany;* orcid.org/0000-0003-3428-039X

Rodrigo Cuevas Arenas − *Interfakultäres Institut für Biochemie, Universität Tübingen, 72076 Tübingen, Germany; Bijvoet Center for Biomolecular Research, Utrecht University, 3584CG Utrecht, Netherlands;* orcid.org/0000-0002-2354-1286

Ana García-Sáez − *Interfakultäres Institut für Biochemie, Universität Tübingen, 72076 Tübingen, Germany; Institut für Genetik, Universität zu Köln, 50931 Köln, Germany*

Frank Schreiber − *Institut für Angewandte Physik, Universität Tübingen, 72076 Tübingen, Germany;* orcid.org/0000-0003-3659-6718

Complete contact information is available at: https://pubs.acs.org/10.1021/acs.langmuir.2c03412

Author Contributions

†These authors contributed equally to this work.

Notes

The authors declare no competing financial interest.

■ ACKNOWLEDGMENTS

The authors gratefully acknowledge the allocation of beamtime as well as the support of Dr. Alexey Kikhney at P12 (PETRA III, Hamburg, Germany) and financial support by the Carl Zeiss foundation.

■ REFERENCES

(1) Fagerberg, L.; Jonasson, K.; von Heijne, G.; Uhlén, M.; Berglund, L. Prediction of the human membrane proteome. *Proteomics* **2010**, *10*, 1141−1149.

(2) Terstappen, G. C.; Reggiani, A. silico In research in drug discovery. *Trends Pharmacol. Sci.* **2001**, *22*, 23−26.

(3) Seddon, A. M.; Curnow, P.; Booth, P. J. Membrane proteins, lipids and detergents: not just a soap opera. *Biochim. Biophys. Acta - Biomembr.* **2004**, *1666*, 105−117.

(4) Bayburt, T. H.; Grinkova, Y. V.; Sligar, S. G. Self-assembly of discoidal phospholipid bilayer nanoparticles with membrane scaffold proteins. *Nano Lett.* **2002**, *2*, 853−856.

(5) Bayburt, T. H.; Sligar, S. G. Membrane protein assembly into Nanodiscs. *FEBS Lett.* **2010**, *584*, 1721−1727.

(6) Morgan, C. R.; Hebling, C. M.; Rand, K. D.; Stafford, D. W.; Jorgenson, J. W.; Engen, J. R. Conformational transitions in the membrane scaffold protein of phospholipid bilayer nanodiscs. *Mol. Cell. Proteom.* **2011**, *10*, M111.010876.

(7) Kijac, A. Z.; Li, Y.; Sligar, S. G.; Rienstra, C. M. Magic-angle spinning solid-state NMR spectroscopy of nanodisc-embedded human CYP3A4. *Biochemistry* **2007**, *46*, 13696−13703.

(8) Hagn, F.; Etzkorn, M.; Raschle, T.; Wagner, G. Optimized phospholipid bilayer nanodiscs facilitate high-resolution structure determination of membrane proteins. *J. Am. Chem. Soc.* **2013**, *135*, 1919−1925.

(9) Denisov, I. G.; Sligar, S. G. Nanodiscs for structural and functional studies of membrane proteins. *Nat. Struct. Mol. Biol.* **2016**, *23*, 481−486.

(10) Mak, P. J.; Gregory, M. C.; Denisov, I. G.; Sligar, S. G.; Kincaid, J. R. Unveiling the crucial intermediates in androgen production. *Proc. Natl. Acad. Sci. U.S.A.* **2015**, *112*, 15856−15861.

(11) Ravula, T.; Hardin, N. Z.; Ramamoorthy, A. Polymer nanodiscs: Advantages and limitations. *Chem. Phys. Lipids* **2019**, *219*, 45−49.

(12) Orwick-Rydmark, M.; Lovett, J. E.; Graziadei, A.; Lindholm, L.; Hicks, M. R.; Watts, A. Detergent-free incorporation of a seven-transmembrane receptor protein into nanosized bilayer Lipodisq particles for functional and biophysical studies. *Nano Lett.* **2012**, *12*, 4687−4692.

(13) Dörr, J. M.; Scheidelaar, S.; Koorengevel, M. C.; Dominguez, J. J.; Schäfer, M.; van Walree, C. A.; Killian, J. A. The styrene-maleic acid copolymer: a versatile tool in membrane research. *Eur. Biophys. J.* **2016**, *45*, 3−21.

(14) Knowles, T. J.; Finka, R.; Smith, C.; Lin, Y.-P.; Dafforn, T.; Overduin, M. Membrane proteins solubilized intact in lipid containing nanoparticles bounded by styrene maleic acid copolymer. *J. Am. Chem. Soc.* **2009**, *131*, 7484−7485.

(15) Oluwole, A. O.; Danielczak, B.; Meister, A.; Babalola, J. O.; Vargas, C.; Keller, S. Solubilization of membrane proteins into functional lipid-bilayer nanodiscs using a diisobutylene/maleic acid copolymer. *Angew. Chemie Int. Ed.* **2017**, *56*, 1919−1924.

(16) Thoma, J.; Burmann, B. M. 'Till You Make It−The Pursuit of Suitable Membrane Mimetics for Membrane Protein Biophysics. *Int. J. Mol. Sci.* **2021**, *22*, 50.

(17) Adão, R.; Cruz, P. F.; Vaz, D. C.; Fonseca, F.; Pedersen, J. N.; Ferreira-da Silva, F.; Brito, R. M.; Ramos, C. H.; Otzen, D.; Keller, S.; et al. DIBMA nanodiscs keep α-synuclein folded. *Biochim. Biophys. Acta - Biomembr.* **2020**, *1862*, 183314.

(18) Grethen, A.; Oluwole, A. O.; Danielczak, B.; Vargas, C.; Keller, S. Thermodynamics of nanodisc formation mediated by styrene/maleic acid (2:1) copolymer. *Sci. Rep.* **2017**, *7*, 1−14.

(19) Oluwole, A. O.; Klingler, J.; Danielczak, B.; Babalola, J. O.; Vargas, C.; Pabst, G.; Keller, S. Formation of lipid-bilayer nanodiscs by diisobutylene/maleic acid (DIBMA) copolymer. *Langmuir* **2017**, *33*, 14378−14388.

(20) Hall, S. C.; Tognoloni, C.; Price, G. J.; Klumperman, B.; Edler, K. J.; Dafforn, T. R.; Arnold, T. Influence of Poly (styrene-co-maleic acid) Copolymer Structure on the Properties and Self-Assembly of SMALP Nanodiscs. *Biomacromolecules* **2018**, *19*, 761−772.

(21) Jamshad, M.; Grimard, V.; Idini, I.; Knowles, T. J.; Dowle, M. R.; Schofield, N.; Sridhar, P.; Lin, Y.; Finka, R.; Wheatley, M.; et al. Structural analysis of a nanoparticle containing a lipid bilayer used for detergent-free extraction of membrane proteins. *Nano Res.* **2015**, *8*, 774−789.

(22) Zhang, R.; Sahu, I. D.; Liu, L.; Osatuke, A.; Comer, R. G.; Dabney-Smith, C.; Lorigan, G. A. Characterizing the structure of lipodisq nanoparticles for membrane protein spectroscopic studies. *Biochim. Biophys. Acta - Biomembr.* **2015**, *1848*, 329−333.

(23) Bjørnestad, V. A.; Orwick-Rydmark, M.; Lund, R. Understanding the Structural Pathways for Lipid Nanodisc Formation: How

Styrene Maleic Acid Copolymers Induce Membrane Fracture and Disc Formation. *Langmuir* **2021**, *37*, 6178−6188.
(24) Xue, M.; Cheng, L.; Faustino, I.; Guo, W.; Marrink, S. J. Molecular mechanism of lipid nanodisk formation by styrene-maleic acid copolymers. *Biophys. J.* **2018**, *115*, 494−502.
(25) Lee, S. C.; Knowles, T. J.; Postis, V. L.; Jamshad, M.; Parslow, R. A.; Lin, Y.-P.; Goldman, A.; Sridhar, P.; Overduin, M.; Muench, S. P.; et al. A method for detergent-free isolation of membrane proteins in their local lipid environment. *Nat. Protoc.* **2016**, *11*, 1149−1162.
(26) Good, N. E.; Winget, G. D.; Winter, W.; Connolly, T. N.; Izawa, S.; Singh, R. M. Hydrogen ion buffers for biological research. *Biochemistry* **1966**, *5*, 467−477.
(27) Blanchet, C. E.; Spilotros, A.; Schwemmer, F.; Graewert, M. A.; Kikhney, A.; Jeffries, C. M.; Franke, D.; Mark, D.; Zengerle, R.; Cipriani, F.; Fiedler, S.; Roessle, M.; Svergun, D. I. Versatile sample environments and automation for biological solution X-ray scattering experiments at the P12 beamline (PETRA III, DESY). *J. Appl. Crystallogr.* **2015**, *48*, 431−443.
(28) Svergun, D. Determination of the regularization parameter in indirect-transform methods using perceptual criteria. *J. Appl. Crystallogr.* **1992**, *25*, 495−503.
(29) Kline, S. R. Reduction and analysis of SANS and USANS data using IGOR Pro. *J. Appl. Crystallogr.* **2006**, *39*, 895−900.
(30) Koppel, D. E. Analysis of Macromolecular Polydispersity in Intensity Correlation Spectroscopy: The Method of Cumulants. *J. Chem. Phys.* **1972**, *57*, 4814−4820.
(31) Vargas, C.; Arenas, R. C.; Frotscher, E.; Keller, S. Nanoparticle self-assembly in mixtures of phospholipids with styrene/maleic acid copolymers or fluorinated surfactants. *Nanoscale* **2015**, *7*, 20685−20696.
(32) Arenas, R. C.; Klingler, J.; Vargas, C.; Keller, S. Influence of lipid bilayer properties on nanodisc formation mediated by styrene/maleic acid copolymers. *Nanoscale* **2016**, *8*, 15016−15026.
(33) Atkins, P.; de Paula, J.*Atkins' Physical Chemistry*, 8th ed; Oxford University Press: Oxford, 2006.
(34) Winter, W. Measurement of suspended particles by quasi-elastic light scattering. *J. Polym. Sci. Polym. Lett. Ed.* **1983**, *21*, 1020−1020.
(35) Skar-Gislinge, N.; Simonsen, J. B.; Mortensen, K.; Feidenhans'l, R.; Sligar, S. G.; Møller, B. L.; Bjørnholm, T.; Arleth, L. Elliptical structure of phospholipid bilayer nanodiscs encapsulated by scaffold proteins: casting the roles of the lipids and the protein. *J. Am. Chem. Soc.* **2010**, *132*, 13713−13722.
(36) Skar-Gislinge, N.; Arleth, L. Small-angle scattering from phospholipid nanodiscs: derivation and refinement of a molecular constrained analytical model form factor. *Phys. Chem. Chem. Phys.* **2011**, *13*, 3161−3170.
(37) Skar-Gislinge, N.; Johansen, N. T.; Høiberg-Nielsen, R.; Arleth, L. Comprehensive study of the self-assembly of phospholipid nanodiscs: what determines their shape and stoichiometry? *Langmuir* **2018**, *34*, 12569−12582.
(38) Atkinson, D.; Smith, H. M.; Dickson, J.; Austin, J. P. Interaction of Apoprotein from Porcine High-Density Lipoprotein with Dimyristoyl Lecithin: 1. The Structure of the Complexes. *Eur. J. Biochem.* **1976**, *64*, 541−547.
(39) Denisov, I. G.; McLean, M. A.; Shaw, A. W.; Grinkova, Y. V.; Sligar, S. G. Thermotropic phase transition in soluble nanoscale lipid bilayers. *J. Phys. Chem. B* **2005**, *109*, 15580−15588.
(40) Zhang, M.; Gui, M.; Wang, Z.-F.; Gorgulla, C.; Yu, J. J.; Wu, H.; Sun, Z.J.; Klenk, C.; Merklinger, L.; Morstein, L.; et al. Cryo-EM structure of an activated GPCR-G protein complex in lipid nanodiscs. *Nat. Struct. Mol. Biol.* **2021**, *28*, 258−267.
(41) Pedersen, J. S. Determination of size distribution from small-angle scattering data for systems with effective hard-sphere interactions. *J. Appl. Crystallogr.* **1994**, *27*, 595−608.
(42) Svergun, D.; Barberato, C.; Koch, M. H. J. CRYSOL - a Program to Evaluate X-ray Solution Scattering of Biological Macromolecules from Atomic Coordinates. *J. Appl. Crystallogr.* **1995**, *28*, 768−773.
(43) Tristram-Nagle, S.; Liu, Y.; Legleiter, J.; Nagle, J. F. Structure of gel phase DMPC determined by X-ray diffraction. *Biophys. J.* **2002**, *83*, 3324−3335.
(44) Pencer, J.; Nieh, M.-P.; Harroun, T. A.; Krueger, S.; Adams, C.; Katsaras, J. Bilayer thickness and thermal response of dimyristoylphosphatidylcholine unilamellar vesicles containing cholesterol, ergosterol and lanosterol: a small-angle neutron scattering study. *Biochim. Biophys. Acta - Biomembr.* **2005**, *1720*, 84−91.
(45) Harding, B. D.; Dixit, G.; Burridge, K. M.; Sahu, I. D.; Dabney-Smith, C.; Edelmann, R. E.; Konkolewicz, D.; Lorigan, G. A. Characterizing the structure of styrene-maleic acid copolymer-lipid nanoparticles (SMALPs) using RAFT polymerization for membrane protein spectroscopic studies. *Chem. Phys. Lipids* **2019**, *218*, 65−72.
(46) Bali, A. P.; Sahu, I. D.; Craig, A. F.; Clark, E. E.; Burridge, K. M.; Dolan, M. T.; Dabney-Smith, C.; Konkolewicz, D.; Lorigan, G. A. Structural characterization of styrene-maleic acid copolymer-lipid nanoparticles (SMALPs) using EPR spectroscopy. *Chem. Phys. Lipids* **2019**, *220*, 6−13.
(47) Orwick, M. C.; Judge, P. J.; Procek, J.; Lindholm, L.; Graziadei, A.; Engel, A.; Gröbner, G.; Watts, A. Detergent-Free Formation and Physicochemical Characterization of Nanosized Lipid-Polymer Complexes: Lipodisq. *Angew. Chemie Int. Ed.* **2012**, *51*, 4653−4657.
(48) Hernandez, L. M. R.; Levental, I. Comparing lipid packing between nanodiscs and native membranes. *Biophys. J.* **2022**, *121*, 485a.

https://doi.org/10.1021/acs.langmuir.2c03412
Langmuir 2023, 39, 2450−2459